Supporting Information

Near-Infrared Luminescence AgPd Alloy Superatomic Clusters

Xiao-Hong Ma[a], Jian-Hua Qin*[b], Fei-Fan Wang[c], Peng Luo[d], Xi-Yan Dong*[cd]

[a]College of Chemistry and Chemical Engineering, Xinyang Normal University, Xinyang 464000, China.
[b]College of Chemistry and Chemical Engineering, Luoyang Normal University, Luoyang 471934, China
[c]Henan Key Laboratory of Crystalline Molecular Functional Materials, and College of Chemistry, Zhengzhou University, Zhengzhou 450001, China.
[d]College of Chemistry and Chemical Engineering, Henan Polytechnic University, Jiaozuo 454000, China.

Corresponding authors: jh_q128105@126.com; dongxiyan0720@hpu.edu.cn

Materials and chemicals.

All the chemicals used in our study were of commercially available reagent grade and were used as received without any additional purification, including silver nitrate ($AgNO_3$), pentafluorobenzenethiol (PFBT), tetrakis(triphenylphosphine)palladium ($Pd(TPP)_4$), sodium borohydride ($NaBH_4$), and triphenylphosphine (TPP). Other reagents and solvents for synthesis were obtained from commercial sources and used without further purification.

Instrumentation.

Powder X-ray diffraction (PXRD) patterns of the samples were recorded on a D/MAX-3D diffractometer. Thermogravimetric analyses (TGA) were performed on a TA Q50 system from room temperature (RT) to 500°C at a heating rate of 10°C/min under a nitrogen atmosphere. Electrospray ionization mass spectrometry (ESI-MS) was recorded on an X500R QTOF spectrometer. X-ray photoelectron spectroscopy (XPS) measurements were carried out using a VG Scientific ESCALAB 250 system with an Al Kα (300 W) X-ray resource. Energy-dispersive spectrometry (EDS) measurement was collected using Zeiss Sigma 500. Inductively coupled plasma mass spectrometry (ICP-MS) measurements were carried out using an iCAP6000 SERIES spectrometer. UV-vis absorption spectra were recorded using a Hitachi UH4150. UV-visible spectrophotometer in the range of 200–800 nm. Steady-state photoluminescence spectra were recorded with an Edinburgh FLS 1000 fluorescence spectrometer. Photoluminescence decay was measured on a HORIBA FluoroLog-3 fluorescence spectrometer equipped with a 355 nm laser operating in time-correlated single-photon counting mode (TCSPC) with a time resolution of 340 μs. The photoluminescence quantum yield (PLQY) was measured using an integrating sphere on a HORIBA Scientific Fluorolog-3 spectrofluorometer.

Single-crystal X-ray diffraction Analysis (SCXRD).

SCXRD measurement was performed on a Rigaku XtaLAB Pro diffractometer with Cu-Kα radiation (λ = 1.54184 Å) at 200 K. Data collection and reduction were performed using the program CrysAlisPro[1-2]. The structures were solved with intrinsic phasing methods (*SHELXS*)[3], and refined by full-matrix least-squares on F^2 using *OLEX2*[4], which utilizes the *SHELXL*-2015 module[5]. Imposed restraints in the least-square refinement of each structure were commented on in the corresponding CIF files. Thus only a general description of the structural refinement strategy is presented here. All non-hydrogen atoms were refined anisotropically, and the hydrogen atoms were included in idealized positions. The imposed restraints in the least-squares refinement of each structure were commented on in the corresponding CIF files. Thus, the remaining electron density was flattened out using the solvent masking protocol inside *OLEX2* which results in a decrease in the final R-value. The crystallographic data are listed in Supplementary Table S1.

Quantum chemical calculations.

The density functional theory (DFT) and time-dependent density functional theory (TD-DFT) calculations were performed with Gaussian 16[6] under the Perdew–Burke–Ernzerhof (PBE) exchange-correlation functional[7] using def2SVP[8] basis set for all-atom. The single-crystal structure was chosen as the initial guess for ground-state optimization, and all reported stationary points were verified as true minima by the absence of negative eigenvalues in the vibrational frequency

analysis. SMD solvent model was applied for TD-DFT calculations. The calculated absorption spectra were obtained from Multiwfn 3.8(dev)[9].

Experimental section

Synthesis of Ag$_{14}$Pd: 10 mg AgNO$_3$ and 5 mg Pd(TPP)$_4$ were first dissolved in a mixture of methanol (2 mL) and dichloromethane (4 mL) at room temperature and stirred for 5 min. 10 μL of PFBT, and 50 mg PPh$_3$ were then added. Then, 1 ml of an aqueous solution of NaBH$_4$ (10 mg/mL) was added quickly to the reaction mixture under vigorous stirring. The solution color immediately changed from a yellow solution to a reddish solution. Then the reaction continued for 4 h at room temperature in the dark. The aqueous phase was then removed. The organic phase was washed several times with water. Red rhombohedral single crystals suitable for X-ray diffraction study were grown with an n-hexane/CH$_2$Cl$_2$ solution for two days. The yield of **Ag$_{14}$Pd** was ~29% (AgNO$_3$ basis). Elemental analysis (%) for evacuated **Ag$_{14}$Pd**: calcd C: 47.74, H: 2.78, S: 3.54; found C: 47.68, H: 2.82, S: 3.58.

The process of 3D printing: First, 50 mg of **Ag$_{14}$Pd** was dissolved in 2 mL of CH$_2$Cl$_2$ and added to 100 mL of photosensitive resin. Then the mixture was stirred continuously for 2 hours in dark conditions. After parameter optimization of the 3D equipment, the 3D patterns of the various macroscopic models were printed with mixed raw materials following the imported digital model.
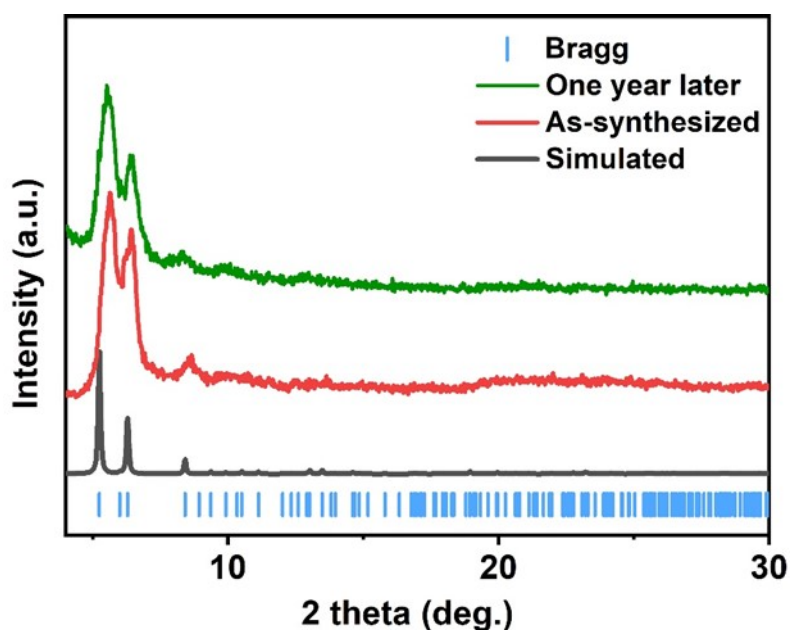

Figure S1. Powder X-ray diffraction patterns patterns of **Ag$_{14}$Pd.**
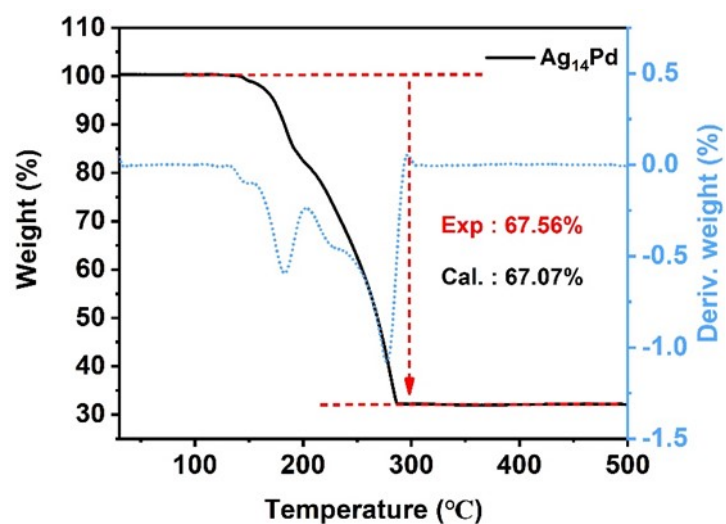
Figure S2. TG curves of **Ag$_{14}$Pd** in N$_2$ atmosphere.

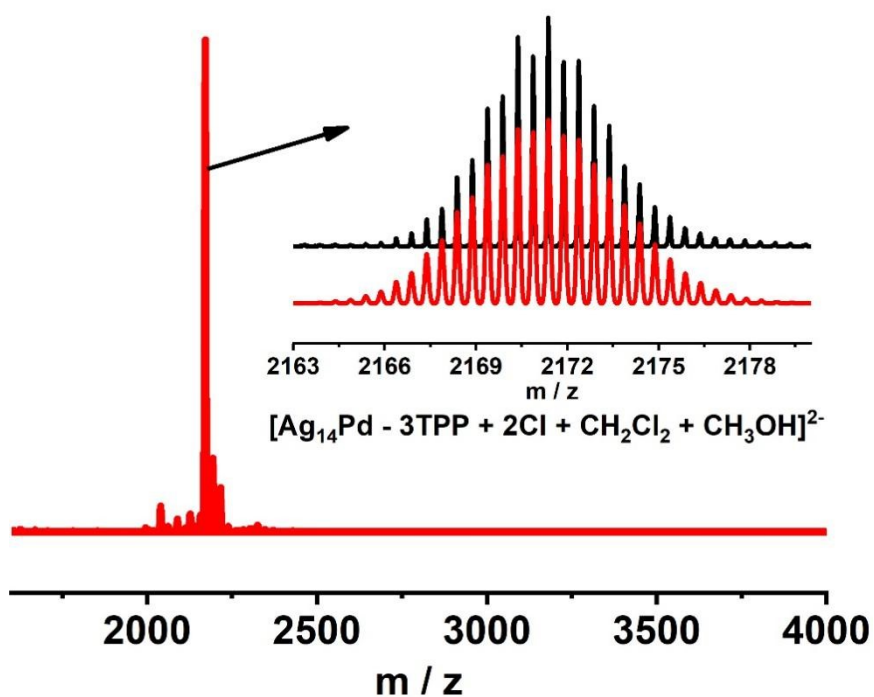[Ag$_{14}$Pd - 3TPP + 2Cl + CH$_2$Cl$_2$ + CH$_3$OH]$^{2-}$

Figure S3. ESI-MS spectra of **Ag$_{14}$Pd** in negative mode. Inset: calculated (black curve) and experimental (red curve) isotope distribution patterns.
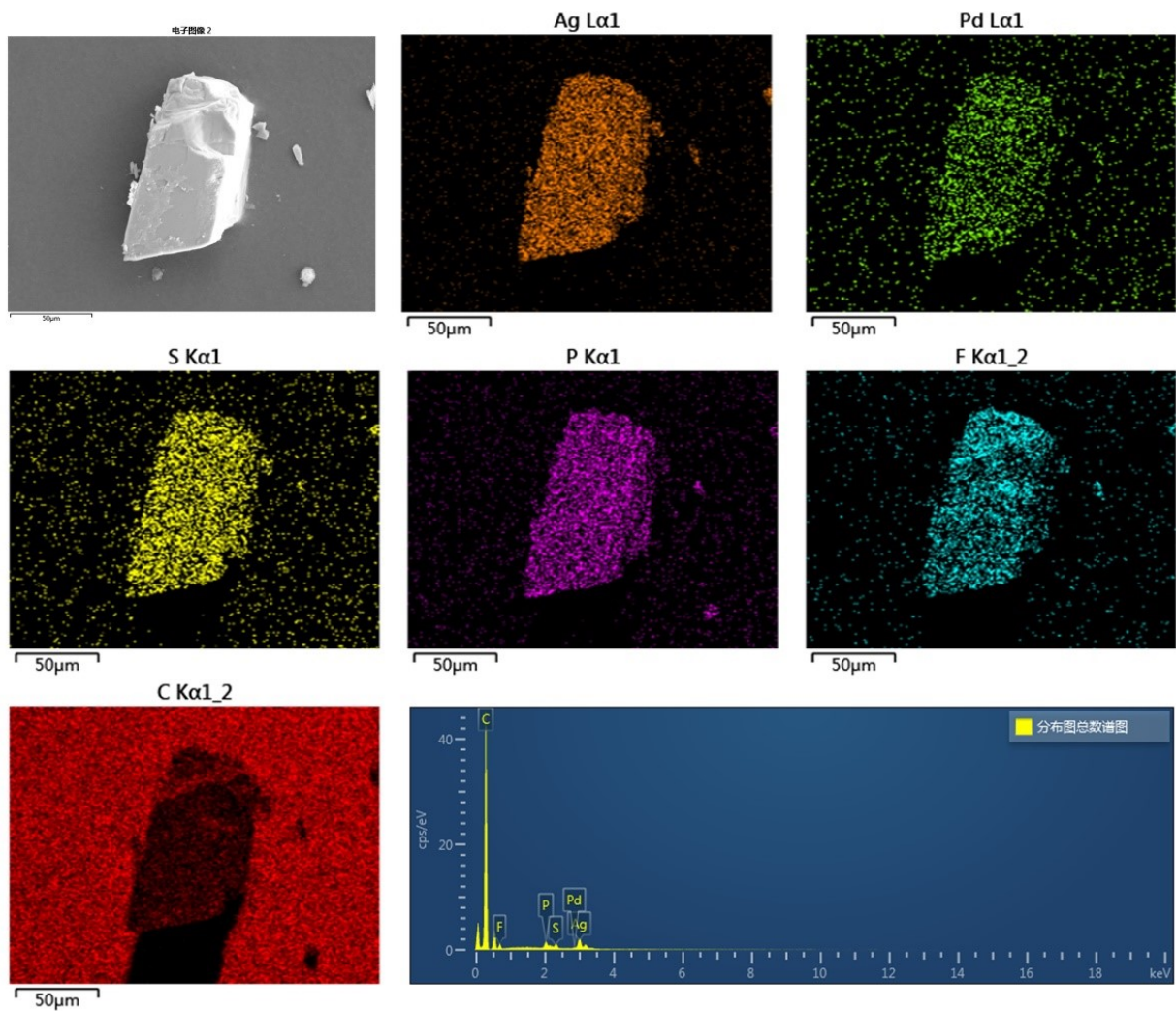
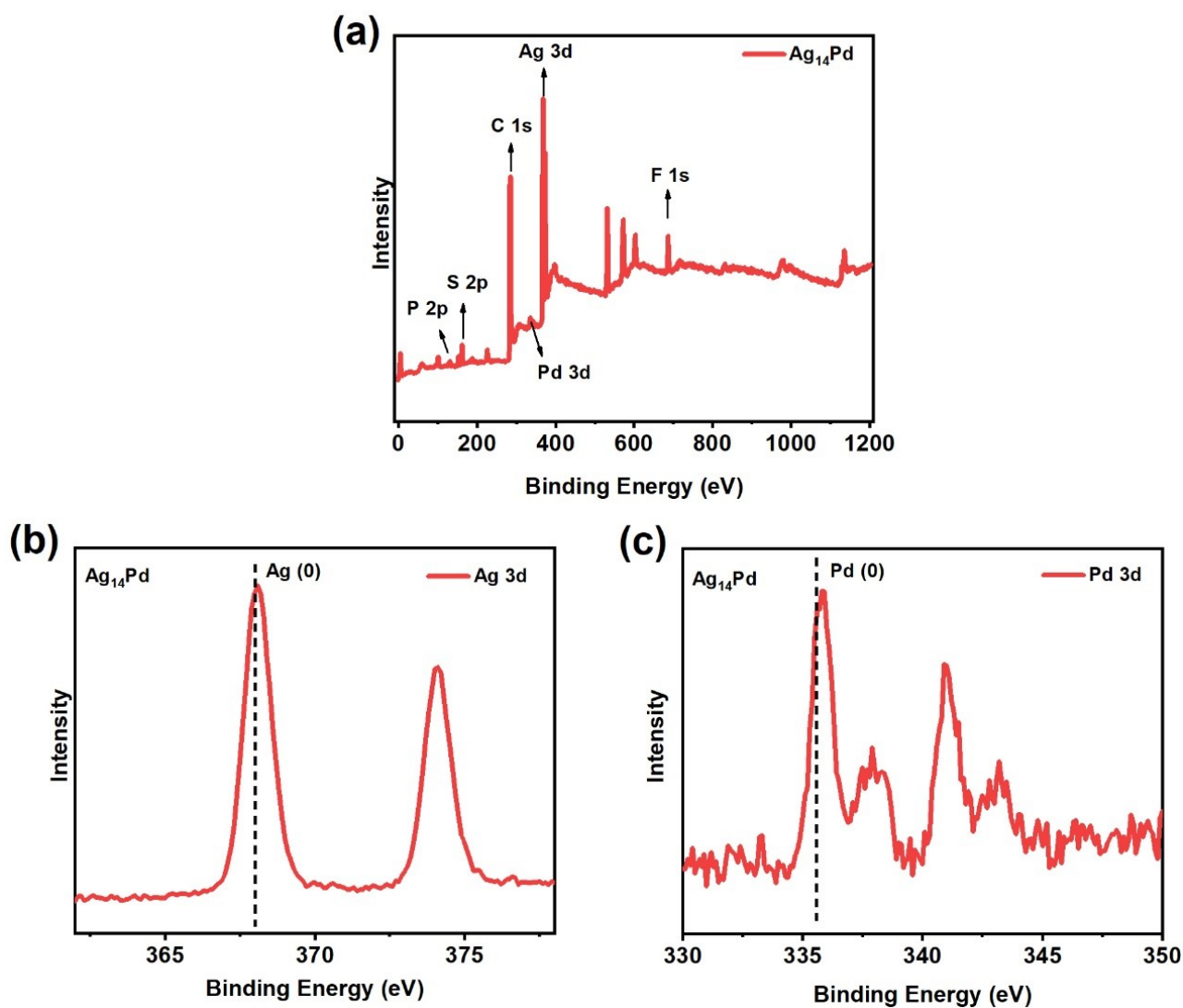**Figure S4.** EDS mapping of **Ag$_{14}$Pd**.

Figure S5. (a) The full XPS spectrum of **Ag₁₄Pd**. The High-resolution XPS spectra of (b) Ag 3d and (c) Pd 3d of **Ag₁₄Pd**.

	Pd (ppm)	Ag (ppm)	Ag : Pd (mol)
Ag₁₄Pd	2.46	34.34	13.96 : 1

Figure S6. ICP-MS analysis of metal contents and calculated ratios in **Ag₁₄Pd**.
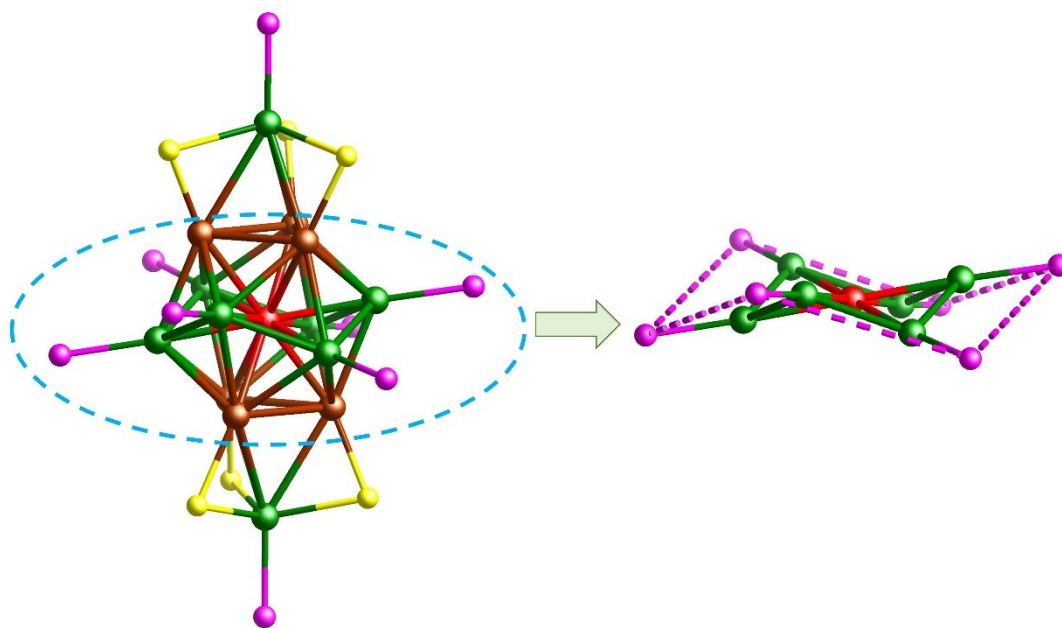
Figure S7. (a) The six S atoms are arranged in cyclohexane-like 'chair' configurations of the **Ag₁₄** core. (b) The types of S−Cu motif.
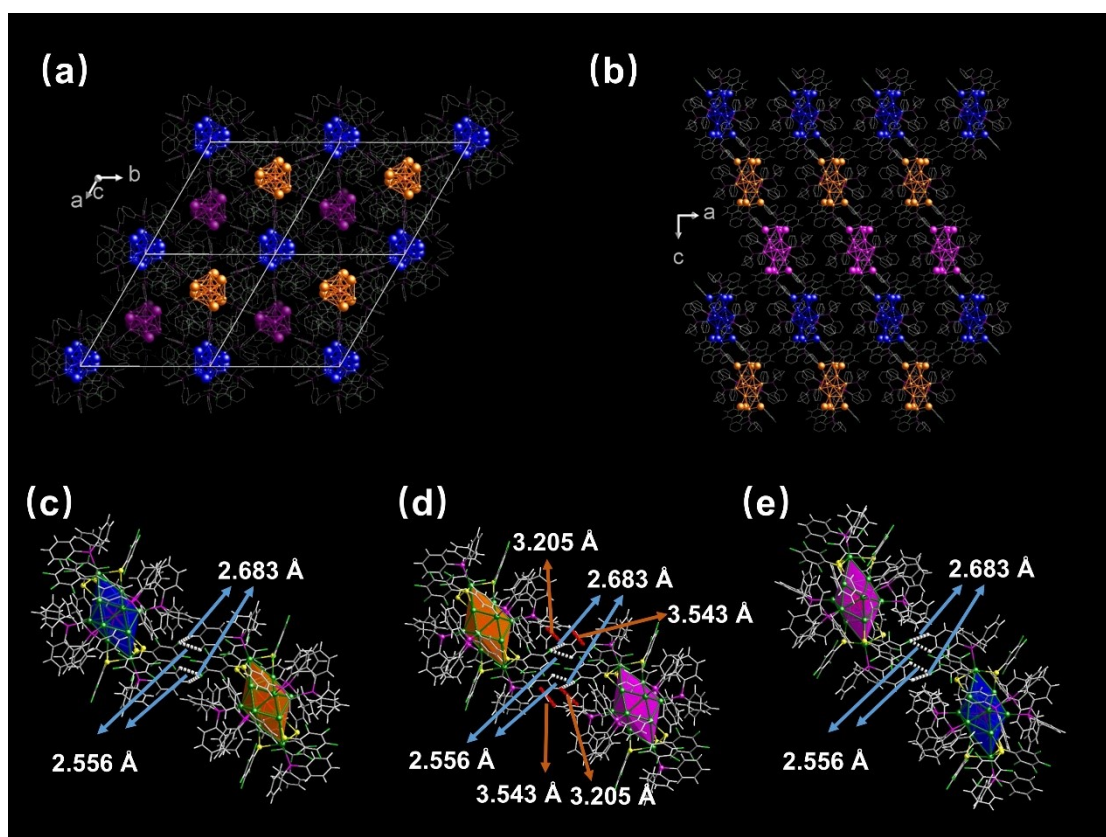

Figure S8. The packing diagram of **Ag₁₄Pd**. View from a direction (a) *c* axis and (b) b axis. (c-e) Intermolecular interactions between clusters of **Ag₁₄Pd**. The red and white dashed lines correspond to the C−H···F and C−H···π interactions, respectively.
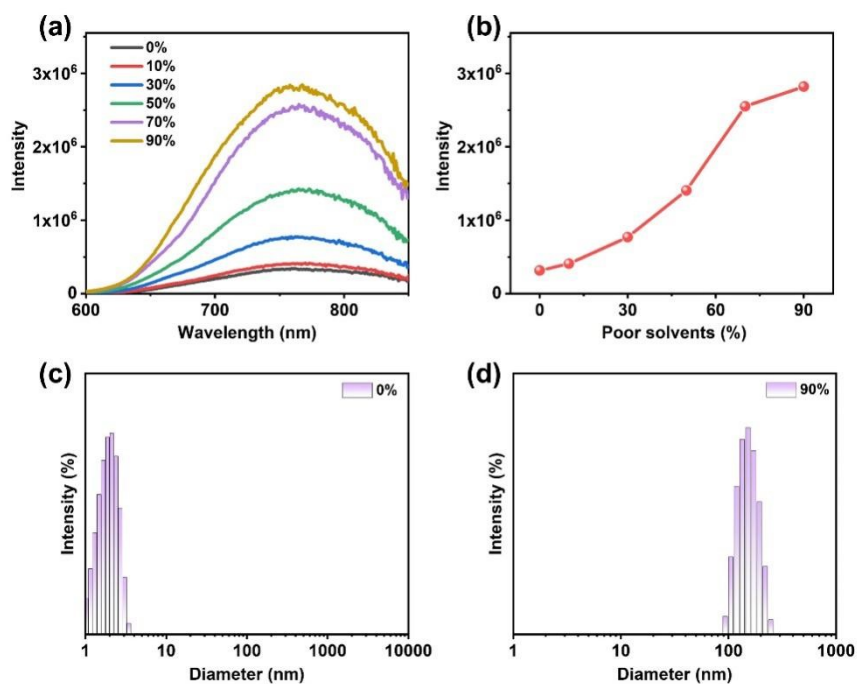
Figure S9. (a) Emission spectra and (b) relative emission intensity of **Ag₁₄Pd** in DCM with different fractions (0%–90%) of hexane. Dynamic light scattering spectra of **Ag₁₄Pd** in DMF with (c) 0% and (d) 80% of n-hexane.
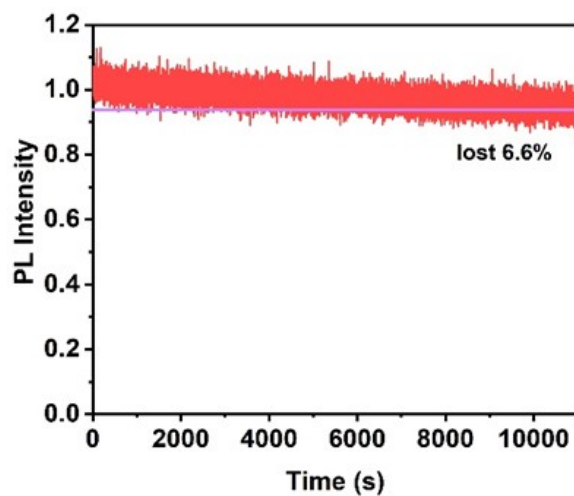

Figure S10. The time-dependent emission intensity of **Ag₁₄Pd** exposure to xenon light irritation for 3 hours in the solid state.
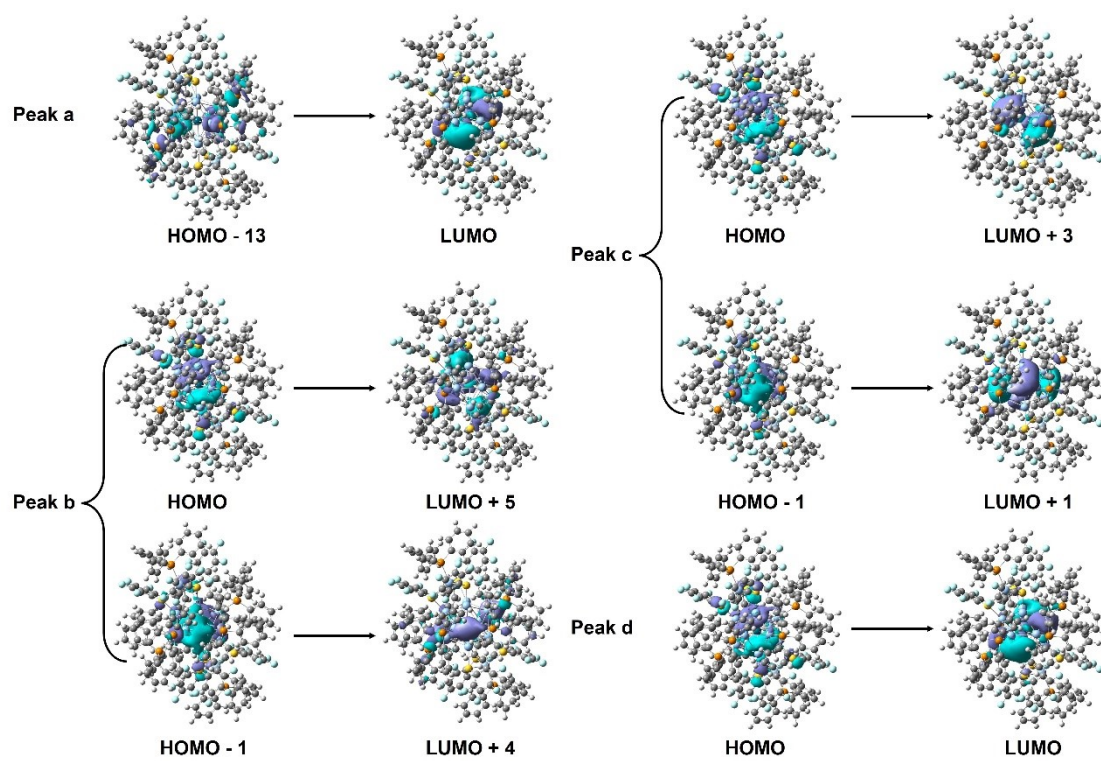
Figure S11 Transition-involved molecular orbitals of **Ag$_{14}$Pd**.

Table S1. Crystal data and structure refinement for **Ag14Pd**

	$Ag_{14}Pd$
CCDC number	2352112
Empirical formula	$C_{216}H_{150}Ag_{14}F_{30}P_{10}PdS_6$
Formula weight	5433.88
Temperature/K	200.00(10)
Crystal system	trigonal
Space group	*R*Error!*c*
a/Å	21.00820(10)
b/Å	21.00820(10)
c/Å	88.3377(5)
α/°	90
β/°	90
γ/°	120
Volume/Å^3	33764.0(4)
Z	6
ρ_{calc} g/cm^3	1.603
μ/mm^{-1}	11.961
F(000)	15996.0
Crystal size/mm^3	0.5 × 0.5× 0.2
Radiation	CuKα (λ = 1.54184)
2θ range for data collection/°	6.294 to 145.098
Index ranges	-25 ≤ h ≤ 18, -17 ≤ k ≤ 25, -106 ≤ l ≤ 54
Reflections collected	36726
Independent reflections	7360 [R_{int} = 0.0364, R_{sigma} = 0.0282]
Data/restraints/parameters	7360/30/417
Goodness-of-fit on F^2	1.034
Final R indexes [I>=2σ (I)]	R_1 = 0.0270, wR$_2$ = 0.0782
Final R indexes [all data]	R_1 = 0.0304, wR$_2$ = 0.0808
Largest diff. peak/hole / e Å^{-3}	0.85/-0.88

$$R_1=\Sigma||F_o| - |F_c||/\Sigma|F_o|, \quad wR_2=[\Sigma[w(F_o^2 - F_c^2)^2]/\Sigma w(F_o^2)^2]^{1/2}$$

Table S2. Selected bond lengths (Å) for **Ag$_{14}$Pd**

Bond lengths (Å)			
Ag1–Ag2[1]	3.2279(3)	Pd1–Ag4[3]	2.76848(17)
Ag1–Ag2	3.2281(3)	Pd1–Ag4[4]	2.76834(17)
Ag1–Ag2[2]	3.2280(3)	Pd1–Ag4[2]	2.76842(17)
Ag2–Ag2[1]	2.8641(3)	Pd1–Ag4[5]	2.76834(17)
Ag2–Ag2[2]	2.8642(3)	Ag4–Ag4[5]	2.9175(3)
Ag2–Pd1	2.74634(16)	Ag4–Ag4[4]	2.8730(3)
Ag2–Ag4[2]	2.8885(2)	Ag1–S1[1]	2.6682(6)
Ag2–Ag4[3]	2.9390(2)	Ag1–P2	2.5229(12)
Ag2–Ag4[3]	2.9107(2)	Ag2–S1	2.4593(5)
Pd1–Ag4[1]	2.76842(17)	Ag4–P1	2.4812(7)
Pd1–Ag4	2.76838(17)		

[1]1 - Y, + X - Y, + Z;[2]1 + Y - X, 1 - X, + Z;[3]1/3 + Y, - 1/3 + X, 7/6 - Z;[4]4/3 - X, 2/3 – X + Y, 7/6 - Z;[5]1/3 – Y + X, 2/3 - Y, 7/6 - Z

References

[1] CrysAlisPro Version 1.171.36.31. Agilent Technologies Inc. Santa Clara, CA, USA, 2012.

[2] CrysAlisPro 1.171.38.41k (Rigaku Oxford Diffraction, 2015).

[3] G. M. Sheldrick, Acta Cryst. A, 2008, **64**, 112-122.

[4] O. V. Dolomanov, L. J. Bourhis, R. J. Gildea, et al., Appl. Cryst. 2009, **42**, 339-341.

[5] G. M. Sheldrick, Acta Cryst. C, 2015, **71**, 3-8.

[6] M. J. Frisch, *et al*. Gaussian, Inc., Wallingford CT, 2016.

[7] J. P. Perdew, K. Burke, M. Ernzerhof, Phys. Rev. Lett. 1996, **77**, 3865–3868.

[8] F. Weigend, R. Ahlrichs, Phys. Chem. Chem. Phys. 2005, **7**, 3297.

[9] T. Lu, F. W. Chen, J. Comput. Chem. 2012, **33**, 580.